Chemical Engineering Science 66 (2011) 163–170

Contents lists available at ScienceDirect

Chemical Engineering Science

journal homepage: www.elsevier.com/locate/ces

MOF-74 building unit has a direct impact on toxic gas adsorption

T. Grant Glover [a,*], Gregory W. Peterson [c], Bryan J. Schindler [a], David Britt [b], Omar Yaghi [b]

[a] SAIC, PO Box 68 Gunpowder, MD 21010, United States
[b] Center for Reticular Chemistry at the California NanoSystems Institute, Department of Chemistry and Biochemistry, University of California-Los Angeles, 607 Charles E. Young Drive East, Los Angeles, CA 90095, United States
[c] Edgewood Chemical and Biological Center, 5183 Blackhawk Road, APG, MD 21010-5424, United States

ARTICLE INFO

Article history:
Received 12 August 2010
Received in revised form
30 September 2010
Accepted 3 October 2010
Available online 11 November 2010

Keywords:
MOF-74
Breakthrough
Adsorption
Packed bed
Porous media
Filtration

ABSTRACT

Metal organic framework (MOF-74) analogs have been synthesized using cobalt, magnesium, nickel, and zinc metal centers. The capability of these materials to remove ammonia, cyanogen chloride, and sulfur dioxide from air has been evaluated via fixed-bed breakthrough testing in both dry and humid conditions. Octane breakthrough tests were performed to determine the physisorption capacities of the materials. All materials were stored in air prior to use. Dynamic breakthrough capacities of the analogs were compared to 13X zeolite and BPL activated carbon. The impact of the metal center on the adsorption behavior is illustrated with each analog providing different ammonia and cyanogen chloride adsorption capacities. The results provide an important step in the assessment of the potential of MOFs to function as porous adsorbent materials.

1. Introduction

Numerous studies have been published in recent years that describe the gas adsorption properties of metal organic frameworks (MOFs), a new class of porous crystalline adsorbent materials. Many of these studies have concentrated on adsorption as a means of storage of fuel gases, such as hydrogen and methane (Duren et al., 2004; Millward and Yaghi, 2005; Vitillo et al., 2008; Wong-Foy et al., 2006). However, one of the most common applications of adsorbent materials are gas separations, where it is important to consider, not only the adsorption equilibria, but also the adsorption kinetics (LeVan et al., 1997; Ruthven, 1984).

The number of studies that have examined dynamic gas separations using MOFs is limited (Britt, et al., 2008, 2009; Hayashi, et al., 2007). Furthermore, publications describing dynamic gas separations in air streams containing water vapor, often the case in practical systems, are almost non-existent (Peterson et al., 2009; Galli et al., 2010). Because the pore structure and functionality of MOFs can be tailored to a specific application, they present an opportunity to separate gases that are difficult for traditional materials, such as activated carbons and zeolites, to separate.

Of the current MOF materials, MOF-74 presents the unique advantage of coordinatively unsaturated (open) metal sites that can be varied without affecting the underlying framework structure (Scheme 1). Thus, it is possible to test the effect of the metal center on the gas separation properties of MOF-74. Caskey et al. utilized this opportunity and examined the gas storage capacity of Zn, Co, Ni, and Mg analogs of MOF-74 (Caskey et al., 2008). Here we report the capability of these analogs (M-MOF-74; M: Zn, Co, Ni, Mg) to remove toxic gases dynamically from air in both dry and humid conditions.

For this particular study, we are concerned with assessing the capability of novel materials to purify breathing air. To that end, we have selected adsorbate gases representing acid adsorbates, sulfur dioxide and cyanogen chloride, as well as a basic adsorbate, ammonia, and a physically adsorbed compound, octane. Although a large number of toxic industrial chemicals exist, such as hydrogen cyanide, phosgene, and others, the set discussed here provides a reasonable sample set to determine if MOF-74 materials can be used for air purification. Also, because we are interested in purifying toxic compounds from breathing air, it is important that we examine low pressure adsorption of the above adsorbates in dynamic conditions.

The results will show that the analogs are able to remove toxic gases in dry environments, that the MOF materials are able to retain the gases that are adsorbed, that water competitively adsorbs with the adsorbates studied, and that the metal site has a direct impact on the gas capacity of the material.

* Corresponding author. Tel.: +1 410 436 9408; fax: +1 410 436 5513.
E-mail address: grant.glover@us.army.mil (T.G. Glover).

0009-2509/$ - see front matter © 2010 Elsevier Ltd. All rights reserved.
doi:10.1016/j.ces.2010.10.002

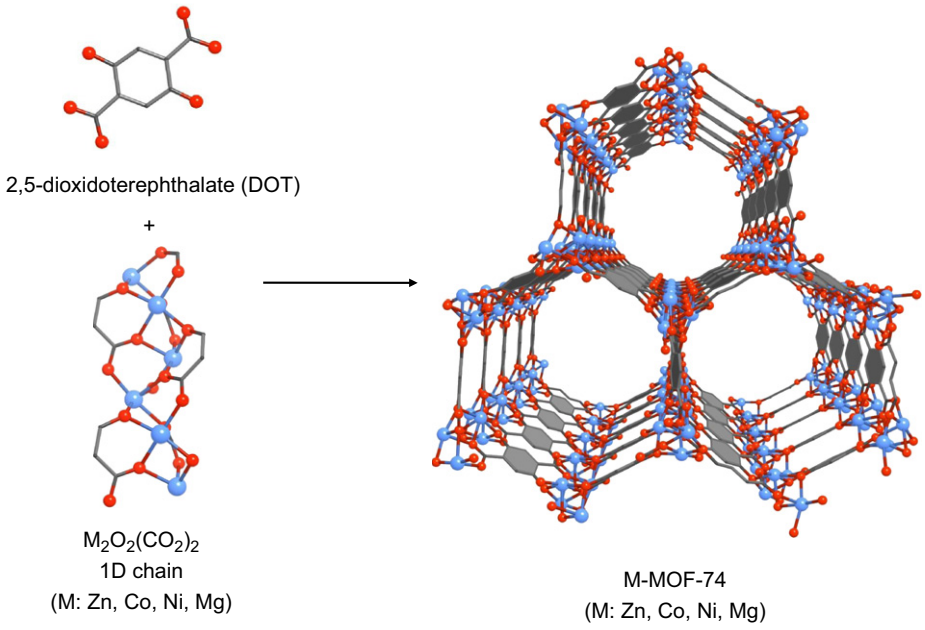

Scheme 1. Synthesis of MOF-74 metal analogs.

2. Materials and methods

2.1. Synthesis procedure

2.1.1. Cobalt MOF-74 (Co-MOF-74)

In a 400 mL jar, with sonication, 0.5 g of 2,5 dihydroxyterephthalic acid (DHTA) and 1.5 g of $Co(NO_3)_2\ 6H_2O$ were dissolved in 70 mL of dimethylformamide (DMF), 70 mL of ethanol, and 70 mL of water. The jar was capped tightly and placed in a 100 °C oven for 2.75 days. After cooling to room temperature, the mother liquor was decanted, the products were washed with methanol, and immersed in methanol. The methanol solvent was decanted and replaced once per day over the next three days. The products were then evacuated to dryness and heated under vacuum to 250 °C. After 24 h, the sample was cooled to room temperature and stored.

2.1.2. Magnesium-MOF-74 (Mg-MOF-74)

With sonication 0.112 g of DHTA and 0.475 g of $Mg(NO_3)_2\ 6H_2O$ were dissolved in 45 mL of DMF, 3 mL of ethanol, and 3 mL of water. The solution was decanted into five 20 mL vials, which were capped tightly and placed in a 125 °C oven for 21 h. After cooling to room temperature, the mother liquor was decanted and replaced with methanol. The products were combined into one batch and the methanol solvent was decanted and replaced five times over the next two days. The sample was evacuated to dryness and heated under vacuum to 250 °C. After 6 h, the samples were cooled to room temperature and stored.

2.1.3. Nickel-MOF-74 (Ni-MOF-74)

In a 400 mL jar, with sonication, 0.5 g of DHTA and 1.5 g of $Ni(NO_3)_2\ 6H_2O$ were dissolved in 70 mL of DMF, 70 mL of ethanol, and 70 mL of water. The jar was capped tightly and placed in a 100 °C oven for 2.75 days. After cooling to room temperature, the mother liquor was decanted and the products washed three times with DMF, three times with methanol, and immersed in methanol. The methanol solvent was decanted and replaced once per day over the next three days. The products were then evacuated to dryness and heated under vacuum to 250 °C. After 5 h, the sample was cooled to room temperature and stored.

2.1.4. Zinc-MOF-74 (Zn-MOF-74)

In a 400 mL jar, with sonication, 1.00 g of DHTA and 4.52 g of $Zn(NO_3)_2\ 4H_2O$ were dissolved in 100 mL of DMF. Then 5 mL of water was added and the solution and sonication was continued. The jar was capped tightly and placed in a 110 °C oven for 21.5 h. After cooling to room temperature, the mother liquor was decanted and the products washed three times with DMF, three times with methanol, and immersed in methanol. The methanol solvent was decanted and replaced once per day over the next three days. The products were then evacuated to dryness and heated under vacuum to 150 °C over a period of 1 h. After 10 h at 150 °C, the heat was increased to 265 °C over a period of 1 h. After 10 h at 265 °C, the sample was cooled to room temperature and stored.

It should be noted that after these materials were synthesized they were stored in a nitrogen environment prior to calculating BET surface area and powder X-ray diffraction analysis. After verifying the structure and porosity of the materials, they were subsequently stored in air under ambient moisture conditions.

2.2. Powder X-ray diffraction (PXRD)

Powder X-ray diffraction data were collected using a Bruker D8-Discover θ–2θ diffractometer in reflectance Bragg–Brentano geometry, employing a Ni filtered Cu Kα line focused radiation at 1600 W (40 kV, 40 mA) power and equipped with a Vantec Line detector. Radiation was focused using parallel focusing Gobel mirrors. The system was also outfitted with an anti-scattering shield, which prevents incident diffuse radiation from hitting the detector, eliminating the normally observed large background at $2\theta < 3°$. Samples were mounted on glass slides by dropping powders from a wide-blade spatula, and then leveling the sample surface with a spatula. Given that the particle size of the 'as synthesized' samples were already found to be quite monodisperse, no sample grinding or sieving was used prior to analysis. We note, however, that the micron sized crystallites lead to peak broadening. The best counting statistics were achieved by collecting samples using a 0.02° 2θ step scan from 1.5° to 60° with an exposure time of 10 s per step. No peaks could be resolved from the baseline for $2\theta > 35°$; therefore, this region was not considered for further analysis.

2.3. Adsorption equilibrium

2.3.1. Nitrogen isotherms

Cryogenic nitrogen isotherm data were collected with a Quantachrome Autosorb Automated Gas Sorption System. Nitrogen isotherm data were used to estimate the surface area and pore volume of the materials.

2.3.2. Water isotherms

Water isotherms at 25 °C were collected using a Cahn microbalance, as shown in Fig. 1. Water was delivered from a saturator cell to a temperature-controlled Cahn balance containing the sorbent to be evaluated. The relative humidity was controlled by adjusting the temperature of the adsorption cell. The equilibrium loading was calculated from the change in the weight recorded by the Cahn microbalance. All materials were stored in air prior to gathering water isotherms.

2.4. Micro-breakthrough experiments

Micro-breakthrough experiments were conducted using the apparatus shown in Fig. 2. Analyte was injected into a ballast and subsequently pressurized; this chemical mixture was then mixed with an air stream containing the required moisture content to achieve a predetermined concentration. The completely mixed stream then passed through a sorbent bed submerged in a temperature-controlled water bath. The sorbent bed is filled on a volumetric basis in a 4 mm internal diameter tube to a height of 4 mm resulting in approximately 20 mg of MOF-74 material being used for each test. The sample bed was constructed of glass, so that the bed height could be measured. The samples were regenerated in dry air at 120 °C for 1 h and humid samples were then pre-humidified in air at 80% relative humidity (RH) at 20 °C for 2 h. To evaluate the desorption behavior of the material after breakthrough had occurred clean air, with the humidity of clean air matching the conditions of the experiment, was passed to the bed. The dry air used in these experiments had a dew point of approximately −35 °C. In all cases, the effluent stream then passed through a continuously operating HP5890 Series II Gas Chromatograph. All of the data were plotted on a normalized time scale of minutes per gram of the adsorbent. Details of the experimental conditions are shown in Table 1.

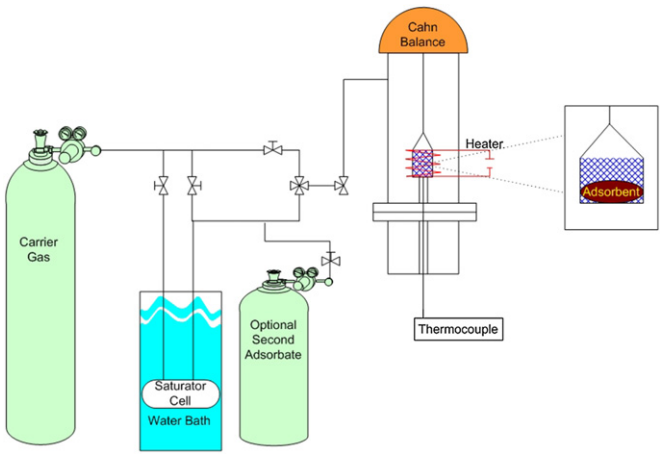

Fig. 1. Water adsorption isotherm system.

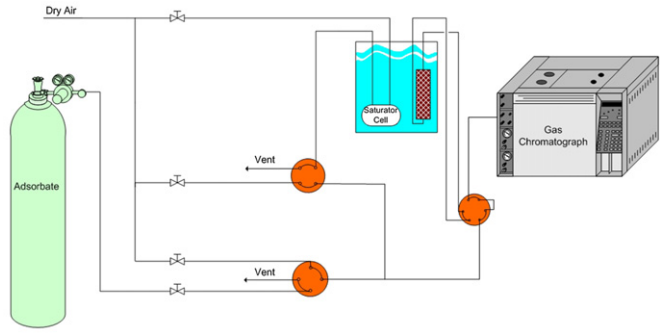

Fig. 2. Rapid nanoporous adsorbent breakthrough testing apparatus.

Table 1
Micro-breakthrough experimental conditions.

Parameter	Values			
	NH_3	CK	SO_2	Octane
Challenge Concentration (mg/m^3)	1000	4000	1000	4000
Temperature (°C)	20			
RH	0, 80%			
Bed height (mm)	4			
Bed volume (mm^3)	50			
Flow rate (ml/min) at 20 °C	20			
RT (s)	0.15			
Detector	GC/PID	GC/FID	GC/FPD	GC/FID

For BPL activated carbon, the samples were regenerated at 150 °C for 1 h. For the humid breakthrough experiments, the samples were then pre-humidified at 80% relative humidity for 2 h. The zeolite 13X samples were regenerated for 150 °C for 24 h, and for the humid breakthrough runs the samples were pre-humidified for 2 h at 80% relative humidity at 20 °C.

To establish a basis for the consistency of the breakthrough device, control breakthrough experiments were performed using dry ammonia and H-ZSM-5 adsorbent. Fifteen control runs were performed over a period of 8 months using approximately 35 mg of adsorbent and a bed height of approximately 4 mm. The average loading of all these tests was 2.2 mol/kg with a standard deviation of 0.2 mol/kg. These control runs provide a high degree of confidence in the repeatability of the breakthrough tests performed on the MOF-74 analogs. Breakthrough tests were also performed on all the breakthrough systems using 20×40 mesh glass beads to ensure that the adsorption bed and system were not influencing the breakthrough behavior. No significant time delay was observed for the glass bead runs, nor was any adsorption observed.

For the breakthrough test involving 13X zeolite regenerated at 350 °C under vacuum, a "dry-bed" was used to ensure the sample was never exposed to air. The dry-bed is comprised of a stainless steel bed, of approximately the same diameter and height as the bed used for all other breakthrough testing, with valves on the inlet and outlet of the bed allowing for the sample to be sealed in the bed. The 13X zeolite was regenerated using an Autosorb 1A outgasser for 22 h and then moved into a glove box, where the Autosorb sample cell was opened and approximately 20 mg of regenerated 13X zeolite was loaded into the dry-bed. In this case, the exact bed height could not be measured; however, from breakthrough experiments with 13X regenerated at 150 °C, it was known that approximately 20 mg would produce a 4 mm bed height. Unlike the other breakthrough runs, this bed was not placed in the water bath, but rather was performed at room temperature. The average temperature was 19 °C and the standard deviation was 1.6 °C during the experiment. Because the dry-bed was a different configuration than previously used, a breakthrough test was completed with ammonia and 20×40 mesh glass beads. The

dry-bed loaded with glass beads showed no significant time delay or adsorption phenomena.

All materials were stored in air prior to use. In most cases, breakthrough tests were run within the same month of synthesis of the MOF material. For the Zn analog, the testing was spread out over a period of 8 months after materials synthesis. For the Mg analog, most breakthrough testing was completed within a month of the synthesis of the material. However, because Mg-MOF-74 was generally synthesized in limited quantities, it was necessary that two additional samples be synthesized and used for testing. Specifically, all Mg analog tests were performed with the same sample, except for the humid ammonia and humid octane. A third sample was used to test humid sulfur dioxide. Although it would be preferred to test all of the materials using the same batch of sorbent, this was not possible due to limited amounts of material and the extensive number of tests performed in this study. Mg was the only analog that required multiple batches to complete the testing. All batches of the Mg analog had similar physical properties in regards to surface area and porosity.

3. Theory

Breakthrough data were used to calculate the dynamic capacity to saturation, using the following equations. First, a concentration-time, or Ct, number is defined as

$$Ct_{feed} = t_f C_{feed} \tag{1}$$

where Ct_{feed} has units of mg min/m^3, t_f is the time that the feed is passed to the system, and C_{feed} is the concentration of the feed in mg/m^3. The Ct eluting from the sorbent until feed termination is calculated by integrating under the elution curve, using the mid-point rule

$$Ct_{elution} = \sum_{t=0}^{ts} \frac{C_n + C_{n-1}}{2}(t_{n-1} - t_n) \tag{2}$$

where $Ct_{elution}$ has units of mg min/m^3, t_s is the time to saturation in minutes, Ct_n is the concentration at time n in mg/m^3, and Ct_{n-1} is the concentration at time $n-1$ in mg/m^3. Eq. (2) is also used when accounting for desorption, or the amount of chemical off-gassing from the sorbent after feed termination. Eq. (3) is used to calculate W_E, the effective loading to saturation, with and without desorption

$$W_E = \frac{(Ct_{Feed} - Ct_{Elution} - Ct_{Desorption})F_{feed}}{M_{ads}MW} 10^{-6} \tag{3}$$

where M_{ads} is the mass of the adsorbent in mg, MW is the molecular weight of the chemical in the feed in mg/mol, F_{feed} is the feed flow rate in m^3/min, and W_E has units of mol/kg. Application of these equations assumes that any analyte that resides downstream of the bed after breakthrough is quickly purged from the system without any effective tailing, and all tailing is attributed to desorption of adsorbate from the porous material. Experimentally, it is assumed that any gas downstream of the bead is quickly swept away as a result of the large flow rate (20 mL/min) relative to the small tubing diameter (1/16″).

4. Results

The XRD results shown in Fig. 3, as well as the nitrogen adsorption isotherms shown in Fig. 4, provide strong evidence that MOF-74 analogs were correctly synthesized. The surface areas of these analogs, shown in Table 2, follow the proper trends in surface area as reported by others (Caskey et al., 2008).

Because the breakthrough results were conducted in both dry and humid conditions, water adsorption isotherms were also measured. All materials were stored in air prior to gathering water isotherms. The results are shown in Fig. 5. The sensitivity of these materials to ambient conditions is also reflected in these isotherms. Specifically, if a MOF analog loses its structural order upon exposure to air, then any isotherms measured after that exposure may reflect lower loading than a material stored under dry conditions. Table 3 summarizes the moisture loadings at three relative humidity conditions. It is clear that MOF-74 analogs adsorb an appreciable amount of water with even the lowest uptake near 0.1 g of water adsorbed per gram of sorbent.

The breakthrough data for the separation of dry ammonia on MOF-74 provide an illustration of the impact the metal site of MOF-74 can have on dynamic filtration (Fig. 6). Based on the dynamic loading calculated from these data, the magnesium and

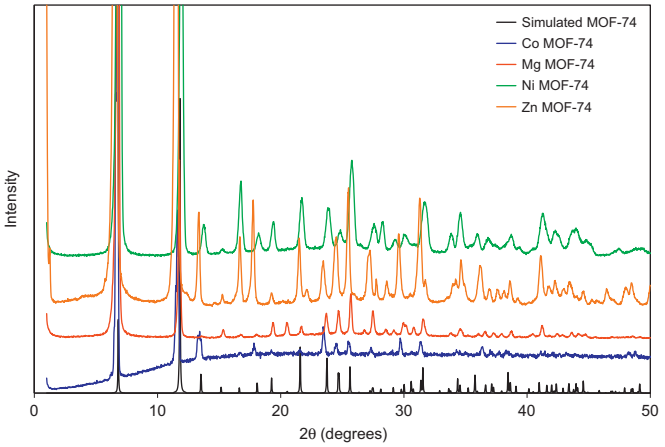

Fig. 3. Powder X-ray diffraction patterns for MOF-74 analogs.

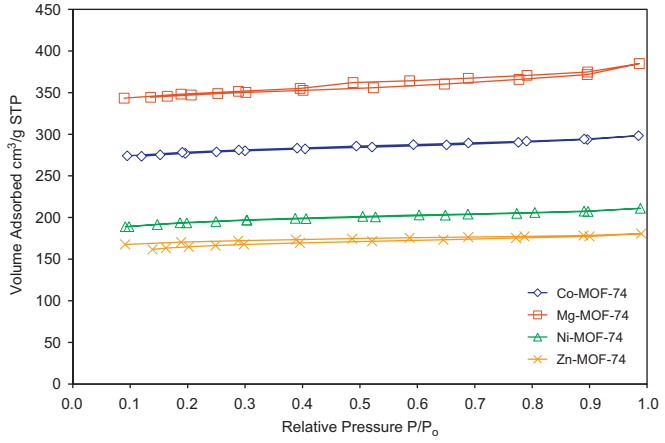

Fig. 4. Nitrogen adsorption isotherms for various MOF-74 materials.

Table 2
BET capacities of MOF-74 analogs.

MOF-74 Analog	BET area
	m^2/g-Adsorbent
Mg-MOF-74	1206
Co-MOF-74	835
Ni-MOF-74	599
Zn-MOF-74	496

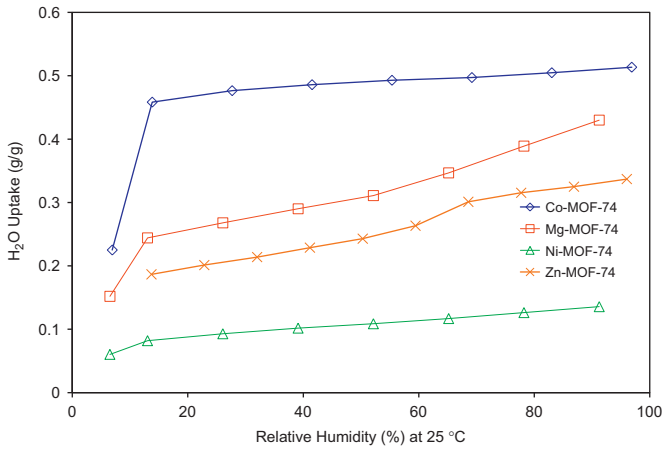

Fig. 5. Water adsorption equilibria at 25 °C for MOF-74.

Table 3
Water loading of sorbents at 25 °C.

MOF-74 analog	Water loading (g-water/g-sorbent)		
	15% RH	50% RH	80% RH
Co	0.46	0.49	0.50
Mg	0.25	0.31	0.39
Ni	0.08	0.11	0.13
Zn	0.19	0.24	0.32

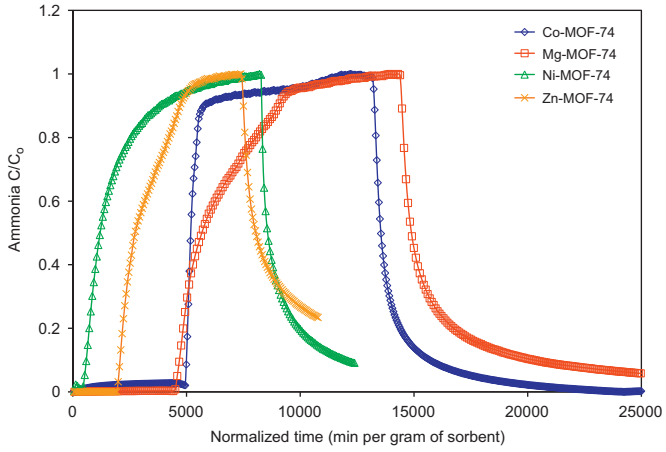

Fig. 6. Breakthrough and desorption curves for dry (RH=0%) ammonia on MOF-74 analogs. Desorption is achieved by passing clean air to the bed at the same temperature and pressure, at which the toxic gas entered the bed.

Table 4
Dynamic loadings of MOF-74 analogs.

Loading (mol/kg)		Metal incorporated in MOF-74			
		Co	Mg	Ni	Zn
Ammonia	Dry	6.70	7.60	2.30	3.70
	Wet	4.30	1.70	1.90	2.80
Cyanogen chloride	Dry	5.60	1.20	2.40	3.60
	Wet	0.05	0.08	0.17	0.10
Octane	Dry	1.90	3.50	1.40	1.20
	Wet	0.05	0.18	0.16	0.05
Sulfur dioxide	Dry	0.63	1.60	0.04	0.26
	Wet	0.03	0.72	0.02	0.04

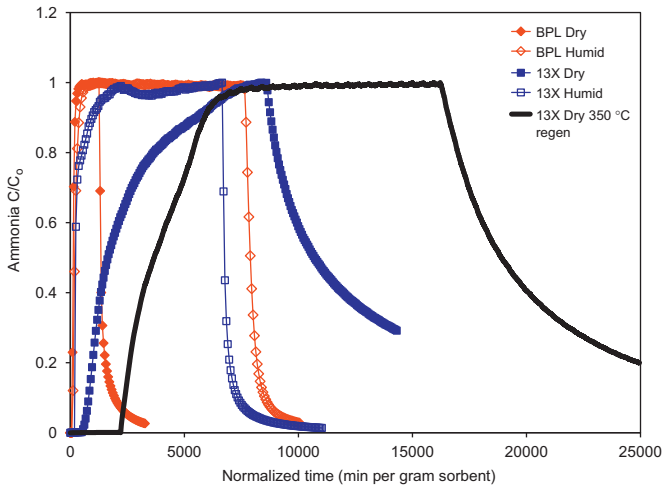

Fig. 7. Breakthrough curves for ammonia on BPL activated carbon, 13X zeolite under dry and humid (RH=80%) conditions, and dry ammonia on 13X zeolite regenerated at 350 °C under vacuum.

Table 5
Dynamic loadings of ammonia on BPL activated carbon and 13X zeolite.

	Sorbent mass*	Loading
	g	mol/kg
BPL carbon (dry)	0.021	0.17
BPL carbon (wet)	0.017	0.29
13X zeolite (dry)	0.019	2.86
13X zeolite (wet)	0.017	0.62

* Dry basis—does not include mass of loaded water.

cobalt materials, with loadings of 7.6 and 6.6 mol/kg, respectively, clearly outperform the nickel and zinc materials (Table 4).

Furthermore, when ammonia is loaded on these materials in dry conditions, a significant portion of the adsorbed ammonia is retained when the materials are exposed to dry air during a desorption experiment (70% and 83% retention by the Co and Mg analogs, respectively). This result is noteworthy because the 13X zeolite, one of the most widely used porous adsorbents, did not retain any of the adsorbed ammonia in dry conditions after desorption under similar breakthrough conditions.

The dynamic loadings of ammonia on all the MOF-74 analogs are generally near to or exceed the maximum loadings of traditional materials, such as 13X zeolite, which has a loading of 2.86 mol/kg when tested under the same conditions, and BPL activated carbon, which has effectively no capacity for dry ammonia. Specifically, in dry conditions Mg-MOF-74 loads nearly three times the capacity of 13X zeolite, and in fact the worst performing analog, Ni-MOF-74, loads at 80% of the capacity of 13X as shown in Fig. 7 and Table 5.

Although the capacity of the MOF-74 analogs is reduced in a humid gas stream, they maintain significant capacity for ammonia in a humid environment as shown in Table 4 and Fig. 8. For example, Mg-MOF-74, the worst performing MOF-74 analog for wet ammonia, has 6 times the capacity of BPL activated carbon, while the best analog, Co-MOF-74, has over 15 times the capacity of BPL and 7 times the capacity of 13X zeolite.

To be thorough, we also regenerated 13X zeolite at 350 °C under a strong vacuum for 22 h. We loaded this sample into the dry-bed sample holder, described above, and performed the dry ammonia

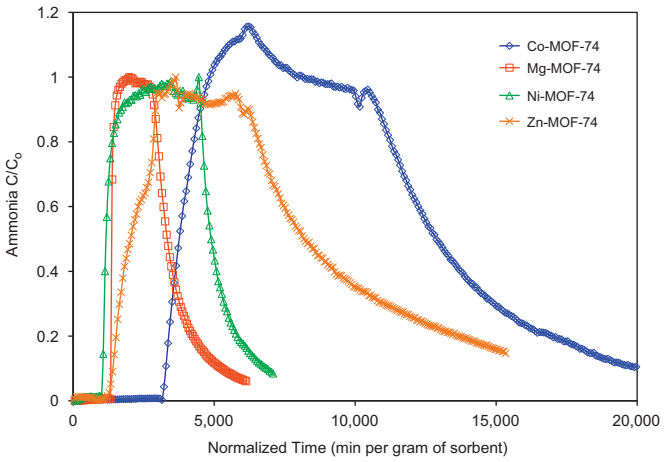

Fig. 8. Ammonia breakthrough curves under humid (RH=80%) conditions.

adsorption experiment again. Under these regeneration conditions, 13X loads 4.77 mol/kg. The Mg-MOF-74 material loads 1.6 times the capacity of 13X zeolite and the Ni-MOF-74 loads at 48% of the capacity of 13X zeolite, when the zeolite is regenerated under these conditions. The 13X gains performance under these regeneration conditions, but significantly more energy is required relative to the MOF samples.

We should note that it is possible to optimize the zeolite structure via an acidification or an ion exchange, which would change the breakthrough performance of the material. However, for this study, 13X zeolite is utilized only to provide a reference for the performance of the materials. Specifically, altering the zeolites may increase capacity, but may also make it difficult to place the performance of the MOF-74 materials in relation to traditional adsorbents.

It is difficult to isolate exactly why one particular metal outperforms another from breakthrough data alone. For example, the ammonia breakthrough data in dry conditions loosely correlates to the surface area of the material; however, in humid conditions this trend does not hold. Because breakthrough data captures material performance, as well as the influence of water, a study focusing exclusively on ammonia adsorption in MOF-74 materials would be necessary to fully determine the roll of each of these metals in the adsorption of ammonia.

In the case of octane, the adsorption behavior is dominated by a physisorption process, and the adsorption breakthrough data are easily correlated to the surface areas of the analogs. Because these materials are porous, the relatively large octane molecules are able to physisorb readily in the pore structure of the material with loadings near 2 mol/kg in dry conditions. In fact, octane is not only adsorbed in dry conditions, but it is also retained during desorption with retention exceeding 62% for all of the analogs. Unlike ammonia, octane shows no appreciable loadings in humid conditions.

The MOF-74 analogs adsorb dry cyanogen chloride well in comparison to traditional materials, with nearly 70% retention by the Co analog even after desorption. However, under humid conditions, all fail to load any appreciable amount of cyanogen chloride. These results are similar to 13X zeolite in both dry and wet conditions.

With the exception of Mg-MOF-74, none of the MOF-74 analogs show any appreciable loading of sulfur dioxide. In general, it is clear from the results in Table 4 that the Co and Mg analogs provide better adsorption of the four gases studied in both dry and humid conditions. Futhermore, it is clear from the table that water vapor has a detrimental effect on the adsorption of these gases on the MOF-74 analogs.

Although breakthrough data do not provide evidence of an adsorption mechanism, if it is assumed that the metal center is the most active adsorption site, an assumption consistent with previous work done on MOF-74 and on other MOF materials, then it is likely that water competes with the toxic gases for the adsorption at the metal center and the competition for the adsorption site leads to diminished breakthrough times and total capacities (Liu et al., 2008; Walton & Snurr, 2007).

We assumed that some degradation of the MOF samples would occur upon storage in air and that these changes would be captured in the breakthrough performance. Although beyond the scope of this work, a separate study is necessary to determine the long term structural stability of these materials when exposed to water.

The strong impact of the metal center underscores the subtle nanoscale control that is possible with MOF chemistry, and the effect is well illustrated by superior ammonia uptake of Co- and Mg-MOF-74 compared to Ni- and Zn-MOF-74 in dry conditions. Also, these results highlight the importance of the interaction of the adsorbate with the metal site. For example, ammonia, which has a Leonard–Jones diameter of 2.6 Å, is well retained by the Co and Mg analogs. However, the octane loadings in both these and the Ni and Zn analogs are much lower in spite of an octane's much larger kinetic diameter.

These results demonstrate that the physisorption process is secondary to strong adsorbent–adsorbate interactions in determining the dynamic loading of toxic gases onto these MOFs. Thus, we propose that an effective strategy for the synthesis of materials that strongly retain one gas in preference to another is to target particular surface chemistry instead of optimizing surface area alone.

5. Conclusions

These breakthrough results document that the MOF-74 series of materials provide a viable means of adsorbing ammonia at capacities and retentions not available in traditional adsorbent media. Octane adsorbs on all the MOF-74 analogs at loadings consistent with the surface area of the materials. Cyanogen chloride loads appreciably onto the Co analog; however, because of the open metal site, water adsorbs competitively and effectively eliminates the capability of MOF-74 analogs to adsorb cyanogen chloride. The competitive adsorption of water is seen on all of the adsorbates examined. Furthermore, although MOF materials have been proposed as highly effective adsorbents, this study provides an important first step in quantifying the capability of these materials to perform separations in realistic environments, particularly in the presence of humidity.

Acknowledgements

The authors thank Amedeo Napolitano, Tara Sewell, Paulette Jones, and John Mahle for their support and the Defense Threat Reduction Agency for funding.

Appendix

Although summarized in the text, the following appendix, comprised of Figs A1–A6 and Tables A1–A5, provides additional details in regards to the breakthrough curves for the chemicals examined.

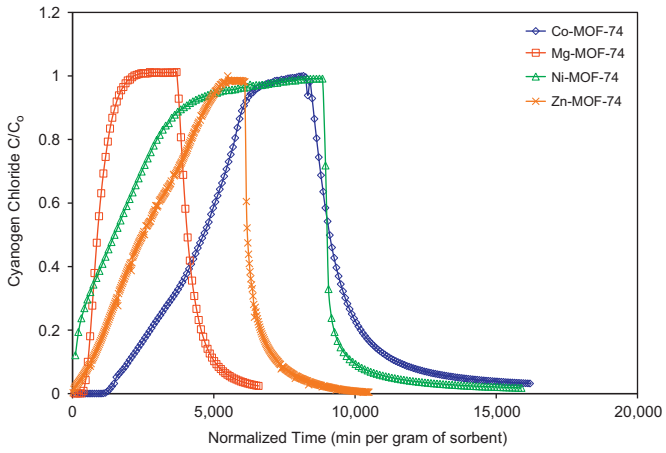

Fig. A1. CK breakthrough curves under dry (RH=0%) conditions.

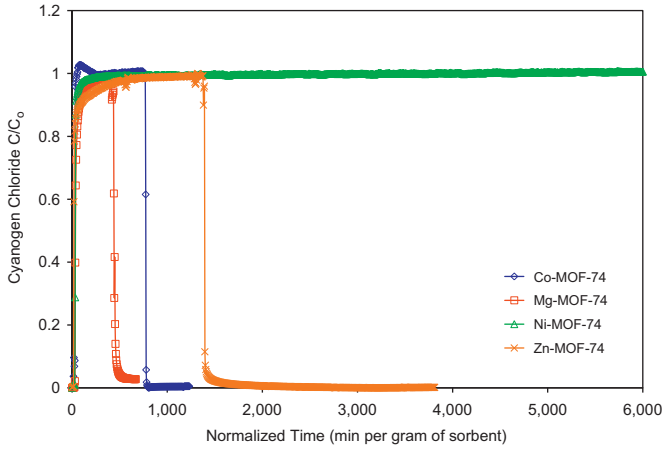

Fig. A2. CK breakthrough curves under humid (RH=80%) conditions.

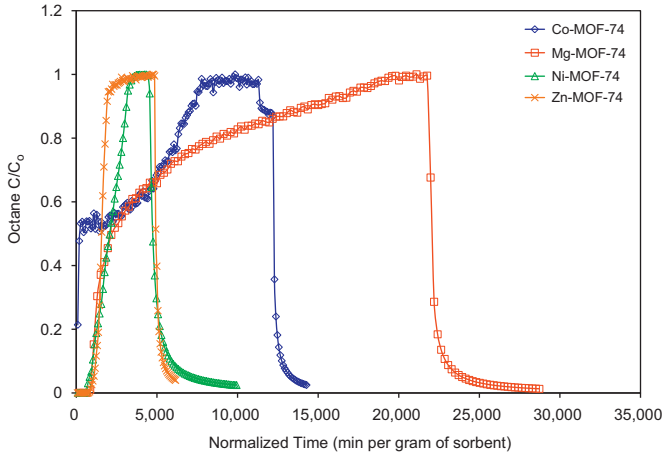

Fig. A3. Octane breakthrough curves under dry (RH=0%) conditions.

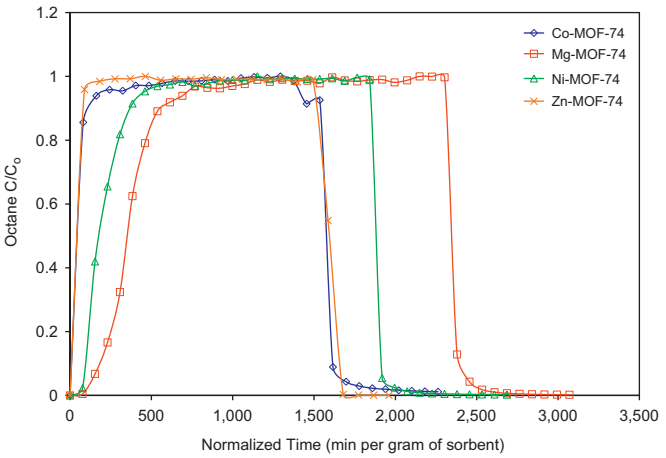

Fig. A4. Octane breakthrough curves under humid (RH=80%) conditions.

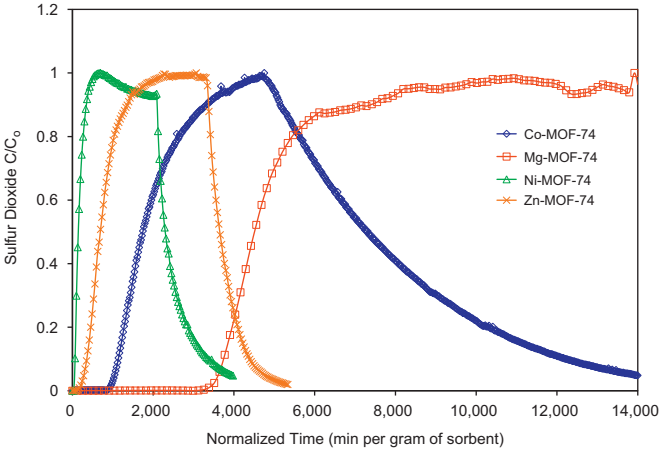

Fig. A5. Sulfur dioxide breakthrough curves under dry (RH=0%) conditions.

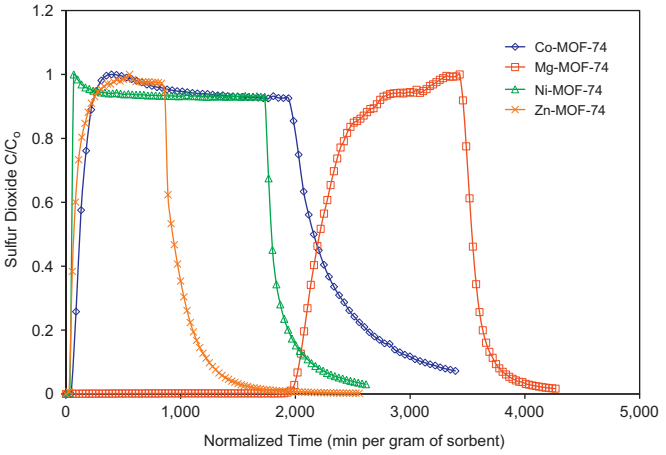

Fig. A6. Sulfur dioxide breakthrough curves under humid (RH=80%) conditions.

Table A1
CK dynamic capacity of sorbents.

MOF-74 analog	Sorbent mass[a]	Effective loading	Effective loading (w/desorption)
	g	mol/kg	mol/kg
Co (dry)	0.0137	5.640	3.940
Co (wet)	0.0113	0.047	0.032
Mg (dry)	0.0136	1.220	0.475
Mg (wet)	0.0125	0.079	0.027
Ni (dry)	0.010	2.400	1.830
Ni (wet)	0.010	0.168	0.123
Zn (dry)	0.0101	3.580	3.090
Zn (wet)	0.0134	0.101	0.081

[a] Dry basis—does not include mass of loaded water.

Table A2
Octane dynamic capacity of sorbents.

MOF-74 analog	Sorbent mass[a]	Effective loading	Effective loading (w/desorption)
	g	mol/kg	mol/kg
Co (dry)	0.0118	1.940	1.220
Co (wet)	0.0132	0.046	0.000
Mg (dry)	0.0049	3.480	2.970
Mg (wet)	0.0217	0.180	0.170
Ni (dry)	0.0103	1.430	1.030
Ni (wet)	0.0139	0.160	0.140
Zn (dry)	0.0156	1.160	1.040
Zn (wet)	0.0114	0.047	0.031

[a] Dry basis—does not include mass of loaded water.

Table A3
Sulfur dioxide dynamic capacity of sorbents.

MOF-74 analog	Sorbent mass[a]	Effective loading	Effective loading (w/desorption)
	g	mol/kg	mol/kg
Co (dry)	0.0229	0.627	0.000
Co (wet)	0.0121	0.032	0.000
Mg (dry)	0.0041	1.560	0.000
Mg (wet)	0.0185	0.716	0.669
Ni (dry)	0.0161	0.035	0.000
Ni (wet)	0.0157	0.020	0.000
Zn (dry)	0.0153	0.256	0.121
Zn (wet)	0.0192	0.039	0.000

[a] Dry basis—does not include mass of loaded water.

Table A4
Ammonia dynamic capacity of sorbents.

MOF-74 analog	Sorbent mass[a]	Effective loading	Effective loading (w/desorption)
	g	mol/kg	mol/kg
Co (dry)	0.0233	6.660	5.540
Co (wet)	0.0149	4.270	0.000
Mg (dry)	0.0123	7.620	5.350
Mg (wet)	0.0193	1.670	0.550
Ni (dry)	0.0161	2.260	1.180
Ni (wet)	0.0170	1.920	1.130
Zn (dry)	0.0182	3.700	2.170
Zn (wet)	0.0176	2.840	0.000

[a] Dry basis—does not include mass of loaded water.

Table A5
Dynamic loadings of BPL activated carbon and 13X zeolite with desorption.

	Sorbent mass*	Loading	Effective loading (w/desorption)
	g	mol/kg	mol/kg
BPL carbon (dry)	0.021	0.17	0.00
BPL carbon (wet)	0.017	0.29	0.00
13X zeolite (dry)	0.019	2.86	0.00
13X zeolite (wet)	0.017	0.62	0.29
13 Zeolite (dry 350 °C regeneration)	0.021	4.77	0.00

* Dry basis—does not include mass of loaded water.

References

Britt, D., Furukawa, H., Wang, B., Glover, T.G., Yaghi, O.M., 2009. Highly efficient separation of carbon dioxide by a metal-organic framework replete with open metal sites. In: Proceedings of the National Academy of Sciences of the United States of America 106, 20637–20640.

Britt, D., Tranchemontagne, D., Yaghi, O.M., 2008. Metal-organic frameworks with high capacity and selectivity for harmful gases. In: Proceedings of the National Academy of Sciences of the United States of America, 105, 11623–11627.

Caskey, S.R., Wong-Foy, A.G., Matzger, A.J., 2008. Dramatic tuning of carbon dioxide uptake via metal substitution in a coordination polymer with cylindrical pores. Journal of the American Chemical Society, 130.

Duren, T., Sarkisov, L., Yaghi, O.M., Snurr, R.Q., 2004. Design of new materials for methane storage. Langmuir 20, 2683–2689.

Galli, S., Masciocchi, N., Colombo, V., Maspero, A., Palmisano, G., Lopez-Garzon, F.J., et al., 2010. Adsorption of harmful organic vapors by flexible hydrophobic bis-pyrazolate based MOFs. Chemistry of Materials 22, 1664–1672.

Hayashi, H., Cote, A.P., Furukawa, H., O'Keeffe, M., Yaghi, O.M., 2007. Zeolite a imidazolate frameworks. Nature Materials 6, 501–506.

LeVan, M.D., Carta, G., Yon, C., 1997. Section 16: Adsorption and Ion Exchange seventh ed. McGraw-Hill, New York.

Liu, Y., Kabbour, H., Brown, C.M., Neumann, D.A., Ahn, C.C., 2008. Increasing the density of adsorbed hydrogen with coordinatively unsaturated metal centers in metal-organic frameworks. Langmuir 24, 4772–4777.

Millward, A.R., Yaghi, O.M., 2005. Metal-organic frameworks with exceptionally high capacity for storage of carbon dioxide at room temperature. Journal of the American Chemical Society 127, 17998–17999.

Peterson, G.W., Wagner, G.W., Balboa, A., Mahle, J., Sewell, T., Karwacki, C.J., 2009. Ammonia vapor removal by Cu-3(BTC)(2) and its characterization by MAS NMR. Journal of Physical Chemistry C 113, 13906–13917.

Ruthven, D., 1984. Principles of Adsorption and Adsorption Processes. Wiley-Interscience, New York.

Vitillo, J.G., Regli, L., Chavan, S., Ricchiardi, G., Spoto, G., Dietzel, P.D.C., Bordiga, S., Zecchina, A., 2008. Role of exposed metal sites in hydrogen storage in MOFs. Journal of the American Chemical Society 130, 8386–8396.

Walton, K.S., Snurr, R.Q., 2007. Applicability of the BET method for determining surface areas of microporous metal-organic frameworks. Journal of the American Chemical Society 129, 8552–8556.

Wong-Foy, A.G., Matzger, A.J., Yaghi, O.M., 2006. Exceptional H-2 saturation uptake in microporous metal-organic frameworks. Journal of the American Chemical Society 128, 3494–3495.